01 Jan 1980

Water And Ice Nucleation Sites From Ion Implantation Of Silicon

William H. Stlnebaugh

Don M. Sparlin
Missouri University of Science and Technology, sparlin@mst.edu

James L. Kassner
Missouri University of Science and Technology

Recommended Citation

W. H. Stlnebaugh et al., "Water And Ice Nucleation Sites From Ion Implantation Of Silicon," *The Journal of Physical Chemistry*, vol. 84, no. 12, pp. 1469 - 1473, American Chemical Society, Jan 1980.
The definitive version is available at https://doi.org/10.1021/j100449a008

Water and Ice Nucleation Sites from Ion Implantation of Silicon

William H. Stinebaugh,* Don M. Sparlin, and James L. Kassner

Graduate Center for Cloud Physics Research, University of Missouri—Rolla, Rolla, Missouri (Received October 1, 1979)

Publication costs assisted by the Graduate Center for Cloud Physics, University of Missouri—Rolla

Ion implantation has a substantial effect on the heterogeneous nucleation of water and ice. An enhancement of water nucleation and a suppression of ice nucleation occurred for samples of silicon implanted with ions of various species and dosage. These effects were noticeable only for samples implanted with ion doses approaching or exceeding the critical dose necessary to produce amorphous silicon. The behavior of the water droplet and ice crystal growth can be related to the amount of ion produced damage to the substrate surface. The nature of the damage can be controlled by variation of the incident ion species, dose, and energy and thus offers a means of quantifying the surface damage while studying its relationship to heterogeneous nucleation.

Introduction

In an effort to study the mechanics involved in the heterogeneous nucleation of water and ice, we have conducted qualitative experiments of heterogeneous nucleation on ion-implanted silicon. Heterogeneous nucleation is one of the most important and at the same time one of the least understood aspects of cloud physics. Since nearly all precipitation from clouds over land masses is initiated by the heterogeneous nucleation of ice on foreign surfaces,[1] an understanding of natural cloud processes and weather modification must begin here. As yet, no comprehensive theory exists relating all the physicochemical properties of chemical compounds (i.e., crystalline structure, water adsorption properties, optical activity, surface structure, etc.) to their nucleating ability. Our aim is to study the nucleation process by using surfaces of well-known characteristics.

Over the past 25 years, rather extensive studies have been conducted concerning the nucleating properties of various substances. Early work attempted to relate the ice-forming properties of nucleants to their crystal similarity with ice and subsequent epitaxial growth.[2] Their limitations became apparent with the discovery of efficient nucleants which were organic compounds[3] and substances of large crystal mismatch with respect to the ice crystal.[4] Although a considerable advance was made in developing a macroscopic theory,[5] a knowledge of the behavior of the nucleation process on the molecular scale is necessary.

The importance of the adsorption properties of water on these substrates has been shown and mechanisms on the molecular scale are being investigated.[6] The existence and effect of active sites is now recognized to be as important as the crystal similarity; however, experimental characterization of these sites is extremely difficult. The difficulty in previous experimental studies of controlling the chemical composition and damage site density led us to pursue a slightly different means to this end.

We have used ion implantation of hydrophobic substrates to study the heterogeneous nucleation processes of water and ice. In order to subject heterogeneous nucleation theory to an experimental test, it is advantageous to induce well-characterized nucleation sites which possess some degree of uniformity and overwhelm the concentration of naturally occurring sites. Ion implantation makes possible the formation of quantified surface damage, ranging from isolated plugs of damage to the production of an amorphous surface layer to the depth of the ion range.[7]

High-energy ion bombardment of the substrate under vacuum produces tracks of ionization damage wherein the local concentration of free valencies associated with broken bonds and misplaced atoms is high. Such sites are preferred for chemisorption and so will attract high concentrations of impurities. We have seen that these impurities or the damage sites themselves play an active role in the heterogeneous nucleation of water and ice on silicon surfaces.

Experimental Section

In order to observe the water droplet and ice crystal growth processes, a cold chamber was assembled. The chamber, similar in design to Layton's[8] (shown in Figure 1) was made of $^1/_4$-in. aluminum with dimensions 4 × 4 × 2 in. and insulated on the outside. The floor of the chamber contained a trough filled with water or ice to provide the necessary saturated vapor within. A small fan operating at low speed stirred the air within the chamber. The temperature of the water or ice reservoir was controlled by three Borg-Warner no. 940-31 thermoelectric units and measured by a transistor thermometer immersed to about the surface level of the water or ice. The samples were placed on an independently controlled thermoelectric unit adjacent to the reservoir. The temperature of the sample was measured by a transistor thermometer situated directly beneath it. The accuracy of the temperatures was estimated to be within 1–2 °C, yielding a rather large error in the calculations of supersaturations; however, our primary concern was observing implant effects, not measuring critical supersaturations. A microscope fitted with a camera was sealed into the chamber for observing the samples. Illumination was provided by an Epoi II fiber optic illuminator containing a dichroic mirror which gave an intense, cold light.

The ion-implanted samples used in our preliminary experiments were borrowed from Dr. E. Hale of our Physics department. They consisted of 20- and 180-keV Li^+, Ar^+, Kr^+, Ne^+, Xe^+, N^+, P^+, N_2^+, and P_2^+ implanted into silicon at doses ranging from 10^{12} to 10^{17} ions/cm^2. The dimensions of the samples were 2 × 1 × 0.1 cm with a masked implanted area of 1.6 × 0.4 cm. This arrangement provided observation of both the implanted region and unimplanted control region adjacent to it.

Each ion-implanted sample was subjected to the same procedure. Distilled water was placed in the reservoir and cooled to the desired temperature. After a sample was placed on the cooling stage, the chamber was sealed, providing a closed environment. The microscope and camera were then focused onto an area of the sample such that a portion of the implanted and unimplanted regions

0022-3654/80/2084-1469$01.00/0

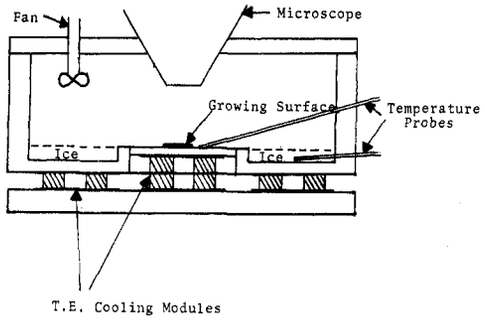

Figure 1. Cutaway view of cold chamber used for observing water and ice nucleation studies on ion-implanted silicon (insulation not shown).

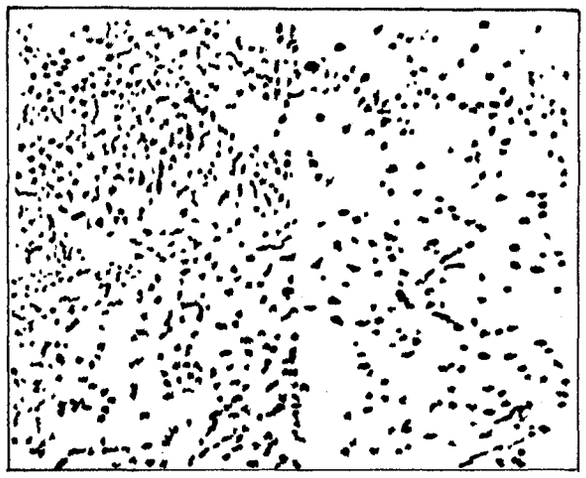

Figure 2. (40X) 20-keV N^+. The dose was 1.5×10^{15} ions/cm^2. The implanted region appears on the left. (This is a trace of the original photograph.)

could be observed simultaneously. The sample was then cooled at a slow rate increasing the supersaturation of the vapor in its vicinity. Photomicrographs were taken at selected intervals during the experiment and the temperature of the sample and reservoir recorded with each picture. At the end of each experiment, the sample was heated to evaporate the water from its surface and the experiment was repeated.

Observations

Experiments were performed on various samples of different ion dose and species which confirmed our belief that ion implantation would affect the nucleation process. Some samples exhibited a pronounced difference in the nucleation and growth habits between the implanted and unimplanted regions. Others exhibited a marginal difference, and some showed no difference.

Water Nucleation. The heterogeneous nucleation of water on ion-implanted samples containing ion doses greater than or equal to the critical dose necessary to form amorphous silicon produced very interesting results. Only at these relatively high doses was a contrast between the two regions noticeable. The appearance of water droplets occurred first on the implanted region at supersaturations of about 10%, and later appeared on the unimplanted region as the supersaturation was increased. In the early stages of droplet growth, a higher density of droplets was visible in the implanted region (Figures 2 and 3, the diameter of the droplets was about 10 μm). Another interesting occurrence was the appearance of a chain of drops along the implanted region's border outlining the boundary between the two regions.

The structure and characteristics of the droplets after they grew were noticeably different between the two regions. The water droplets in the implanted region were generally larger, more irregular in shape, and spaced farther apart. In contrast, they were smaller, rounder, and closer together in the unimplanted portion (Figure 4). The observed contact angle of the water droplets in the implanted region was 15–20° lower than in the unimplanted region.

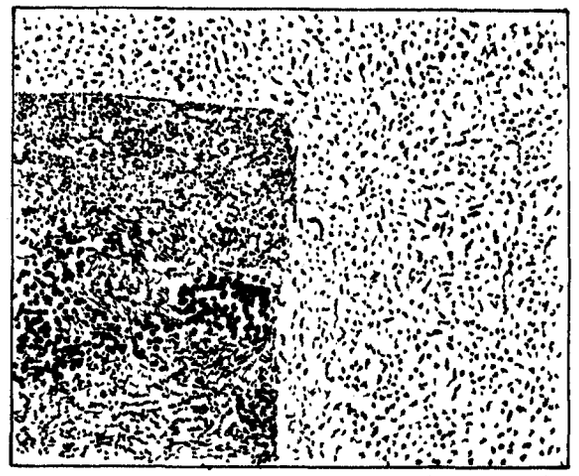

Figure 3. (16X) 20-keV Kr^+. The dose was 6×10^{14} ions/cm^2. The implanted region appears on the left. (This is a trace of the original photograph.)

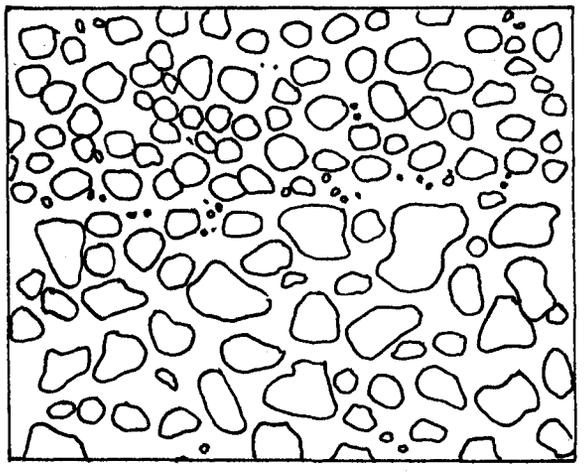

Figure 4. (40X) 20-keV N^+. The dose was 2.4×10^{14} ions/cm^2. The lower portion of the photo is the implanted region. (This is a trace of the original photograph.)

Generally, the results were reproducible after the water was evaporated off and the cooling procedure repeated. Occasionally, a peculiarly interesting pattern appeared in the implant region during the second cooling process. Isolated, large droplets surrounded by surface fog appeared in the implanted region, while normal small droplets formed in the unimplanted zone.

Ice Nucleation. As with water nucleation, the effects of the ion-implanted region were noticeable only for ion doses approaching or exceeding the critical dose, D_0, necessary to produce amorphous silicon. Ice crystals generally appeared first in the unimplanted region and only after increasing the supersaturation would they appear in the implanted region. The ice crystals began to appear at about −20 °C amid water droplets. At cooler temperatures, below −24 °C, ice crystals formed in the absence of any visible water droplets. These observations seem to concur with previous work[2a,f,g9] that, at warmer temperatures, saturation with respect to water is necessary for ice crystals to form; however, at cooler temperatures ice crystals appeared when the vapor was supersaturated

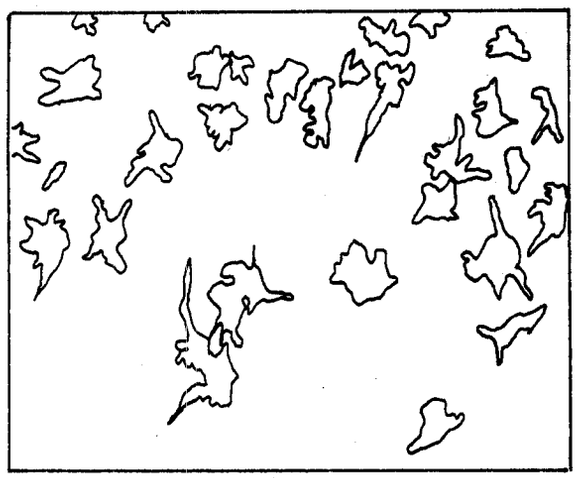

Figure 5. (20×) 20-keV N_2^+. The dose was 6×10^{15} ions/cm^2. The lower portion of the photo is the implanted region. (This is a trace of the original photograph.)

TABLE I: Critical Doses, D_0, Necessary to Produce Amorphous Silicon[13]

ion	energy, keV	(Brice calculation) 10^{14} ions/cm^2	(obsd) 10^{14} ions/cm^2
Li^+	20	12	15
	180	31	40
N^+	20	3.2	2.5
	180	7.4	6.0
Ne^+	20	2.3	2.0
	180	3.8	4.0
Ar^+	20	0.9	1.2
	180	1.3	1.4
Kr^+	20	0.52	0.45
	180	0.45	0.30

(around 20% for our case) with respect to ice but undersaturated with respect to water.

The characteristics and quantity of the ice crystals were generally different between the two regions also. At warmer ice reservoir temperatures (−14 to −19 °C) polycrystalline ice formed in the implanted region while individual ice crystals formed in the unimplanted region. At cooler temperatures (below −20 °C) individual ice crystals grew in both regions but were larger yet fewer in the implanted portion (Figure 5). Some preferred direction was noticeable among the ice crystals in the unimplanted region indicating partial epitaxy while none was noticeable in the implanted zone.

Discussion

Our observations, although qualitative in nature, indicate a general trend which can be explained by examining the processes involved. In essence, we observed a difference in the nucleating characteristics between the ion-implanted and unimplanted regions only for ion doses approaching or exceeding the "critical" dose. This dose is the experimentally determined one which produces amorphous silicon. The critical doses for several ions used in this study are shown in Table I. At ion doses sufficiently below this critical dose, no difference in the nucleation characteristic of the two regions was observed. Since the ion dose is related to the damage inflicted to the surface (i.e., higher dose yields more surface damage), we essentially have witnessed a change in nucleation efficiency that depends on the amount of damage inflicted to the surface. The amount of surface damage can be related to the ESR signal of the surface. Figure 6 shows a typical ESR signal vs. dose plot; the plateau portion represents the formation of amorphous silicon. In an attempt to

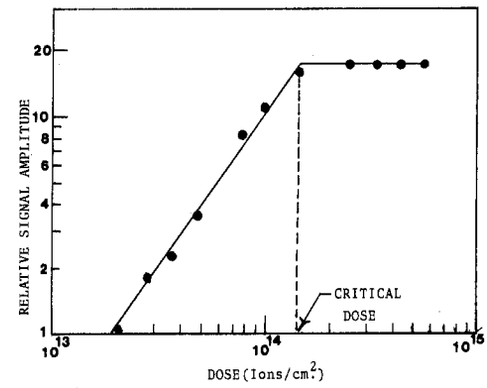

Figure 6. A typical ESR signal vs. ion dose for 180-keV Ar^+.[13] (Note: The ESR signal and surface damage increase until the critical dose, and then level off.)

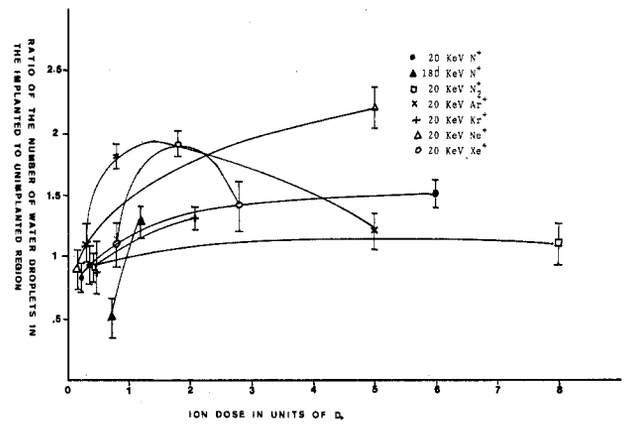

Figure 7. The ratio of the number of water droplets observed in the implanted to unimplanted regions as a function of the critical dose for several ions.

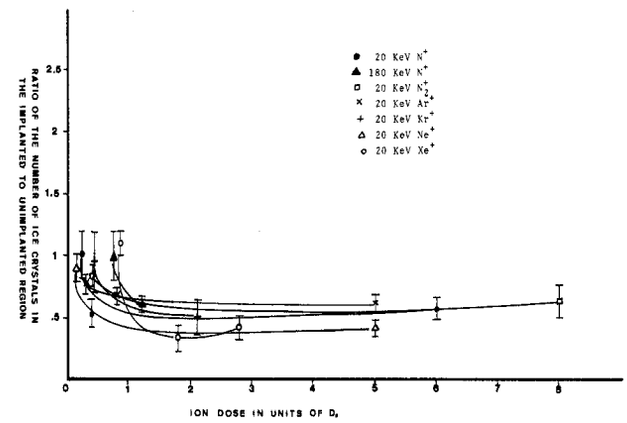

Figure 8. The ratio of the number of ice crystals observed between the implanted and unimplanted regions as a function of the critical dose for several ions.

quantify our data, we counted on a grid the number of ice crystals and water droplets in both the implanted and unimplanted regions. The water droplets were counted at an early state of growth. The ice crystals were counted toward the end of their growth. We then took the ratio of the average number counted per grid square in the implanted to unimplanted regions and plotted them. The results are shown in Figures 7 and 8. Notice the similarity with the ESR vs. dose curve of Figure 6. The inflection occurs around one D_0, the critical dose. Note that both the nucleation density and the ESR damage signals seem to level off into a plateau region at doses above D_0.

Water Nucleation. Our results seem to indicate that ion implantation of the silicon substrate increases the hydroxylation and, thus, the water vapor adsorption as

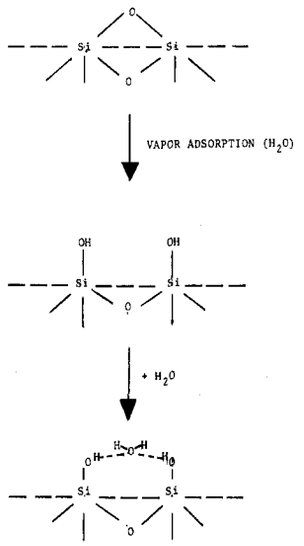

Figure 9. Chemisorption of hydroxyls and subsequent physisorption of water on silica surfaces.[11]

discussed by Kiselev.[10] The high-energy incident ions produce an increased number of unshared bonds as compared to the unimplanted region. These bonds are available for the chemisorption of hydroxyls (H_2O) from the atmosphere. Hydroxylation makes the surface more hydrophillic, reducing the contact angle as we have observed. As we increase the supersaturation of the vapor, water molecules readily physisorb onto the chemisorbed hydroxyls as explained by Zettlemoyer[11] (Figure 9).

The implanted region, therefore, has the greater number of sites for accommodating the physisorbed water molecules, in agreement with the observed enhanced water nucleation region. In addition, scanning electron microscope photographs depicted the ion-implanted region as noticeably "darker" than the unimplanted region. We propose that the decrease in the emission of secondary electrons from the ion-implanted substrate is due to the increased hydroxyl coverage.

The curious chain of droplets which occurred along the implant border was due to the same effects. We usually observed a "dead" region or bare space in the unimplanted zone immediately adjacent to this chain of water droplets. The enhancement of water nucleation in the implanted region tends to scavenge any water droplets which form within a short distance of its boundary, which tends to buildup those droplets along the boundary between the two regions and leaves a barren zone extending into the unimplanted region.

Ice Nucleation. The production of a hydrophillic amorphous region by means of ion implantation decreases the ice nucleation efficiency. It has been shown that efficient nucleants contain hydrophillic sites in a hydrophobic matrix[12] rather than in predominantly hydrophillic surfaces. Our ion-implanted regions are essentially hydrophillic surfaces, with the contact angle decreasing with ion bombardment. Secondly, the mismatch between the lattice parameters of the ice crystal and the substrate increases as the amorphous surface is formed, since the long-range crystalline structure is destroyed. These factors tend to retard the formation of ice crystals in the implanted region as we have observed.

More ice crystals appear in the unimplanted region than the implanted region because the lattice mismatch with ice is lower. Since the long-range crystalline structure of the unimplanted region is not affected, more ice crystals nucleate at a warmer temperature than in the implanted

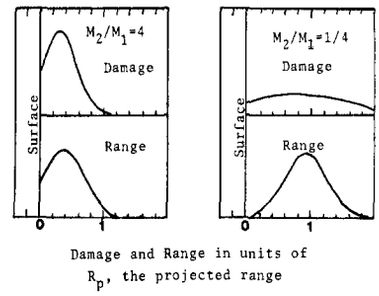

Figure 10. Examples of computed range and damage profiles for substrate to ion mass ratios of 4 and 1/4.[7b]

portion. A relatively low threshold temperature, −11 °C, is expected since the lattice mismatch between ice and a real, oxide covered silicon surface, −15%, is large compared to the mismatch for most effective ice nucleants. The observation that the ice crystals grew larger in the implanted region is assumed to be due to the higher water adsorption there.

Conclusion

We have shown that ion implantation damage has a pronounced effect on the heterogeneous nucleation of water and ice. In general, as the amount of damage to the substrate surface increased, water nucleation was enhanced and ice nucleation suppressed. A known relation exists between the ion dose, species, and energy and the maximum damage possible for the surface, i.e., D_0 (Z,E). Ion implantation offers a means of quantifying the surface damage (Figure 10) in a way not previously applied to nucleation studies of interest in cloud physics.

Future work will concentrate on more quantitative measurements and the production of ion-implanted samples more conducive to cloud physics interests (i.e., F^+ implanted into graphite). A cold chamber is being constructed which will provide more accurate temperature measurements and control, and, thus, more control of the supersaturation within the chamber. In this way, we hope to study the nucleation process in more quantitative detail in a search for new insights into the microscopic nature of the active sites.

References and Notes

(1) N. H. Fletcher, "Physics of Rain Clouds", Cambridge University Press, London, 1962.
(2) (a) G. W. Bryant, J. Hallett, and B. J. Mason, *Phys. Chem. Solids*, **12**, 189 (1959); (b) D. Turnbull and B. Vonnegut, *Ind. Engl. Chem.*, **44**, 1292 (1952); (c) B. J. Mason and J. Hallett, *Nature (London)*, **177**, 681 (1956); (d) B. J. Mason and J. Hallett, *Ibid.*, **179**, 357 (1957); (e) B. J. Mason and J. Maybank, *Q. J. R. Met. Soc.*, **84**, 235 (1958); (f) B. J. Mason and A. van der Heuvel, *Proc. Phys. Soc.*, **74**, 744 (1959); (g) F. S. Harris, D. C. Sparks, and R. G. Layton, *J. Atmos. Sci.*, **20**, 149 (1963); (h) J. Hallett, *Phil Mag.*, **8**, 1073 (1961).
(3) (a) M. Komabayashi and Y. Ikebe, *J. Met. Soc. Jpn.*, **39**, 82 (1961); (b) N. Fukuta and B. J. Mason, *J. Phys. Chem. Solids*, **24**, 715 (1963); (c) R. B. Head, *Nature (London)*, **191**, 1058 (1961).
(4) A. C. Zettlemoyer and K. Kller, *J. Atmos. Sci.*, **34**, (6), 957 (1973).
(5) N. H. Fletcher, Proceedings of the International Conference on Cloud Physics, Tohyo and Sapporo, 1965, p 458.
(6) (a) N. Tcheurekdjian, A. C. Zettlemoyer, and J. J. Chessick, *J. Phys. Chem.*, **68**, 773 (1964); (b) M. L. Corrin and J. A. Nelson, *Ibid.*, **72**, 643 (1968); (c) M. L. Corrin, H. W. Edwards, and J. A. Nelson, *J. Atmos. Sci.*, **21**, 565 (1964); (d) V. G. Morachevsky, N. A. Dubrovich, A. G. Popov, and A. N. Potanin, *J. Rech. Atmos.*, **6**, 371 (1972); (e) V. G. Morachevsky and N. A. Dubrovich, *J. Atmos. Sci.*, **33**, 1989 (1976).
(7) (a) G. Dearnaley, J. H. Freeman, R. S. Nelson, and J. Stephan, "Ion Implantation", North Holland Publishing Co., Amsterdam, 1973. (b) P. D. Townsend, J. C. Kelly, and N. E. W. Hartley, "Ion Implantation Sputering, and Its Applications", Academic Press, London, 1976.
(8) R. G. Layton and J. Steger, *J. Atmos. Sci.*, **26**, (3), 518 (1969).
(9) R. G. Layton and F. S. Harris, *J. Atmos. Sci.*, **20**, 142 (1962).
(10) A. V. Kiselev and V. I. Lygin, "Infrared Spectra of Surface Compounds", Keter Publishing House, Jerusalem, 1975, Chapters IV 2-4, and VII 1.

(11) A. C. Zettlemoyer and E. McCafferty, *Croat. Chem. Acta*, **45**, 173 (1973).
(12) (a) A. C. Zettlemoyer, N. Tcheurekdjian, and C. L. Hosler, *Z. Angew. Math. Phys.*, **14**, 496 (1963); (b) A. C. Zettlemoyer, presented at the 155th National Meeting of the American Chemical Society, San Francisco, Calif., Apr 1–2, 1968.
(13) J. R. Dennis, Ph.D. Thesis, University of Missouri—Rolla, Rolla, MO, 1976. J. R. Dennis and E. B. Hale, *J. Appl. Phys.*, **49** (3) (Mar 1978).

Theoretical Studies of Water Adsorbed on Silver Iodide†

Barbara N. Hale,* Jerry Kiefer, Sergio Terrazas,‡ and Richard C. Ward

Department of Physics and Graduate Center for Cloud Physics Research, University of Missouri—Rolla, Rolla, Missouri 65401

(Received October 1, 1979)

Publication costs assisted by the National Science Foundation

Optimal binding energy contours are generated for H_2O adsorbed on the iodine basal face of β-AgI with a four atomic layer ledge and on the silver basal face with a potassium impurity substituted in a surface silver atom site. The unrelaxed AgI substrate and the (rigid) adsorbed water molecule interact via effective pair potentials which include coulomb, repulsive and attractive short range, and induced dipole terms.[1] An ST-2 four point charge model[2] is used for the water molecule and the AgI substrate is modeled with an infinite array of point atoms with 0.6 e effective charge; an Ewald summation is applied to the coulomb interaction. Results for the ledge and the K impurity are compared with previous results for H_2O adsorption on the smooth surfaces, an I vacancy on the iodine basal face, and a two layer ledge.[1] All the defects produce strong binding sites for the H_2O on the basal face, but give optimal binding energies only slightly larger than the maximal binding energy sites on the smooth prism face. This suggests that the prism faces, or portions of the prism face exposed by steps, compete with impurities and other defects for adsorption of the H_2O. Defect sites could, however, promote formation of icelike water clusters by allowing reorientation of the H_2O dipole moment from that preferred on the smooth substrates. As was found for the smooth surfaces, the K impurity and the four layer ledge favor interstitial adsorption sites—at positions not continuing the bulk AgI structure. Studies of a six water molecule cluster interacting with the iodine basal face of AgI are also presented. Preliminary Monte Carlo calculations indicate the effect of the substrate in restructuring the cluster.

I. Introduction

In an attempt to study on a molecular level the adsorption and nucleation of ice on substrates, we have investigated the optimal binding energy surfaces of a single water molecule on AgI substrates using a microscopic model for the H_2O–AgI interaction. Silver iodide is chosen because of its well-known ice nucleating efficiency and because of its small lattice mismatch with ice I_h. The effective potentials used for the H_2O–AgI interaction were developed by Hale and Kiefer in a study of the water molecule adsorbing on smooth AgI surfaces.[1] The present work examines the effect of a four atomic layer ledge on the iodine basal face of AgI and a potassium impurity on the silver basal face. These studies were made to evaluate modifications of the potential functions and to investigate properties of surface sites promoting adsorption of H_2O. An additional consideration is the ability of the surface site to orient the adsorbed H_2O in configurations leading to formation of icelike clusters.

II. The Model Substrate and the Interaction Potentials

The AgI substrates are modeled by an infinite array of point charge atoms in the wurtzite structure. The lattice parameters $a = 4.58$ Å and $c = 7.494$ Å[3] and an effective charge on the Ag and I atoms of 0.6 e are used.[4] The water molecule is represented by the four point charge ST-2 model of Stillinger[2] and remains rigid in the calculations. The AgI substrate is also assumed to be unrelaxed and rigid. The effective pair potential functions for the H_2O–AgI interaction are as described by Hale and Kiefer[1] and as given below.

$$V = V_{1j} + V_{el} + V_{ind} \tag{1}$$

where

$$V_{1j} = \sum_m 4\epsilon_{mW}\left[\left(\frac{\sigma_{mW}}{|\mathbf{r}_0 - \mathbf{r}_m|}\right)^{12} - \left(\frac{\sigma_{mW}}{|\mathbf{r}_0 - \mathbf{r}_m|}\right)^{6}\right] \tag{2}$$

$$V_{el} = \tfrac{1}{2}\sum_i \sum_m Q_i Q_m / |\mathbf{r}_i - \mathbf{r}_m| \tag{3}$$

and

$$V_{ind} = -\tfrac{1}{2}\sum_n^{\infty}\sum_m^{\infty}\alpha_W\left[\frac{Q_n Q_m(\mathbf{r}_0 - \mathbf{r}_n)\cdot(\mathbf{r}_0 - \mathbf{r}_m)}{|\mathbf{r}_0 - \mathbf{r}_n|^3|\mathbf{r}_0 - \mathbf{r}_m|^3}\right] - \tfrac{1}{2}\sum_n^{\infty}\sum_i^4\sum_j^4\alpha_n\frac{Q_i Q_j(\mathbf{r}_i - \mathbf{r}_n)\cdot(\mathbf{r}_j - \mathbf{r}_n)}{|\mathbf{r}_i - \mathbf{r}_n|^3|\mathbf{r}_j - \mathbf{r}_n|^3} \tag{4}$$

Here the n and m sums are over the surface Ag and I atoms; i and j sums run over the four charges of the water molecule. Q_n, α_n, and $\mathbf{r}_n$ are the effective charge, polarizability, and position vector of the nth atom in the AgI substrate; Q_i, α_W, and $\mathbf{r}_0$ are the ST-2 charge, polarizability, and center of mass position vector of the water molecule, respectively.

†Supported in part by the Atmospheric Research Section, National Science Foundation Grant ATM 77 12614 and in part by NASA Grant 8 31150.
‡CONACYT Fellow, Mexico.

0022-3654/80/2084-1473$01.00/0